Stress fields around magma chambers influenced by elastic thermo-mechanical deformation: implications for forecasting chamber failure

J. Browning[1, 4*], Ö. Karaoğlu[2], Ö. Bayer[3], M. B. Turgay[3], V. Acocella[5]

[1]Department of Mining Engineering and Department of Structural and Geotechnical Engineering, Pontificia Universidad Católica de Chile, Santiago, Chile

[2]Eskişehir Osmangazi University, Department of Geological Engineering, 26040 Eskişehir, Turkey

[3]Department of Mechanical Engineering, Middle East Technical University, Çankaya, Ankara, 06800, Turkey

[4]Centro de Excelencia en Geotermia de los Andes (CEGA), Chile

[5]Dipartimento di Scienze, Università Roma Tre, Rome, Italy

[*]Correspondence and requests for materials should be addressed to J.B. (email: jbrowning@ing.puc.cl)

Keywords: Stress fields, magma chambers, finite element methods, thermoelasticity

Main points:

- Comparison of crustal stresses induced from mechanical and thermomechanical loading around a magma chamber
- Thermal expansion acts to increase the level of shear stress but suppresses the level of tensile stress around pressurized magma chambers
- Elastic deformation resulting from thermal expansion of rocks surrounding magma chambers should be considered in failure forecasting models

Abstract

Defining the conditions that lead to the rupture of a magma chamber is essential to forecast eruptions. So far, models simulating magma chamber dynamics have neglected the effects of elastic thermal expansion in the host rocks surrounding a new injection of magma, focusing instead primarily on elastic-plastic deformation and more recently, on visco-elastic deformation. Here we fill this gap by building a suite of elastic thermo-mechanical models to determine the stress field around a variably heated crustal magma chamber. We first consider linear elastic mechanical models with only the effect of magma pressure. We then present purely thermal models simulating heat distribution around a heated chamber. Finally, we present coupled linear elastic thermo-mechanical models that highlight the influence of temperature on the distribution of crustal stresses. Results show that thermal expansion induced stresses generate two competing consequences: 1) they increase the level of shear stress around the magma chamber and 2) they partially suppress the level of tensile stress generated by the magmatic pressure. These competing effects influence the short-timescale conditions required for the failure of immature magmatic systems and hence the nucleation of dikes which may

ultimately feed eruptions during unrest. Therefore, soon after a new magmatic recharge event, the contribution of temperature increase in the host rocks, following the new influx of magma into a crustal magma chamber, should be considered.

1 – Introduction

Magma emplaced or stored in the crust exerts both mechanical and thermal stresses on the surrounding host rocks (Marsh, 1989). Whilst the stresses and related strains and deformation resulting from mechanical loading are well constrained (i.e. Mogi, 1958; Gudmundsson, 2012), the stresses and deformation resulting from thermo-mechanical loading are less-well understood. It is now well-known that when rocks heat they develop internal thermal strains associated with elastic expansion of the constituent minerals/grains (Fredrich and Wong, 1986; Browning et al., 2016). This thermal expansion of the constituent grains can locally form compressional and/or shear stresses at the grain interfaces which can in turn produce inelastic deformation in the form of crack nucleation and propagation (Fredrich and Wong, 1986). Thermal cracking has been shown to substantially change both the physical and mechanical properties of rock materials (David et al., 1999). However, models that aim to assess the conditions for magma chamber rupture do not usually consider these elastic thermal expansion effects (e.g. Marti et al., 1994; Grosfils, 2007; Grosfils et al., 2015; Karaoğlu et al., 2016), despite the stark contrasts in temperature between hot magma emplaced in relatively cool crustal segments. Indeed, models either neglect the temperature effect, or make the assumption that thermal strains are inherently considered in purely elastic analysis (Gudmundsson, 2011). There have been attempts to analyze the effect of visco-elastic deformation, as opposed to linear-elastic deformation in crustal segments hosting magma chambers (i.e. Maeda, 2000; Del Negro et al., 2009). This seems reasonable since the temperature at which magma is emplaced or stored in the crust likely exceeds the glass transition in many cases, and hence deform viscously (Murase, 1963). However, at some distance from a new magma intrusion or a magma chamber or very soon after the new magma has been emplaced, the rock mass will likely only experience temperatures that encourage it to behave elastically (Castagna et al., 2018). As such, models are needed to test the influence of elastic thermal deformation on the crustal stresses surrounding magma intrusions.

In purely elastic models, forecasting the nucleation of fluid pressure induced mechanical rupture, leading to dike or sill initiation, depends predominantly on the geometry of the magma body, external boundary loading effects and the internal fluid pressure (Browning et al., 2015; Drymoni et al., 2020; Gudmundsson, 2011; Gudmundsson, 2012; Rivalta et al., 2019). Indeed, the rocks around the pressurized magma body are often assumed to deform elastically or plastically, but with apparently little consideration of the elastic response to temperature changes induced by the influx of heated magma. In the simplest, or classical, sense a magma chamber roof will rupture when (e.g. Gudmundsson, 2011; Gudmundsson., 2012; Browning et al., 2015; Gudmundsson., 2020):

$$P_l + P_e = \sigma_3 + T_0 \quad (1)$$

where P_l is the lithostatic or overburden pressure (due to the weight of the overlying rocks), P_e is the magmatic excess pressure within the chamber, σ_3 is the local minimum compressive principal stress and T_0 is the local tensile strength of the host rock. As σ_3 is a local stress, at the margin of the chamber, stress concentration effects due to magma-chamber shape and loading are automatically accounted for in Equation 1. Typical values of tensile strengths for rocks range from 0.5 MPa to 6 MPa and it follows from Eqn. 1 that for any part of the chamber to fail

in tension the local value of P_e reaches T_o. At any other time, the chamber can be considered to be in equilibrium with the surrounding host rock. The effects of thermal expansion or contraction should also be accounted for in this general consideration, but are often neglected. So, the questions become; 1) what is the thermoelastic response of the rocks surrounding a recently emplaced intrusion in terms thermal expansion and thermal stressing and how does this response alter the crustal stress field? 2) Can this response impact the level of P_e required for magma chamber rupture?

In a few models, it has been postulated that 'thermal halos' surrounding bodies of magma can influence the deformation behavior of the rocks and encourage visco-elastic rheological behaviors (e.g., de Silva and Gregg, 2014; Hickey et al., 2016). For example, visco-elastic crustal relaxation does suitably explain decadal volcano deformation signals (e.g., Novoa et al., 2019; Townsend et al., 2019) that relate either to the growth or cooling contraction of large magma bodies. Visco-elastic crustal segments have also been invoked to understand the size of eruption feeding magma chambers (e.g., Degruyter et al., 2016; Townsend and Huber, 2020), but they do not consider the initial failure of the magma body in any clear way. However, in terms of understanding the initial rupture of the rocks surrounding a magma body, which is required for the initiation of a dike, the vast majority of models are purely elasto-plastic. Those that do consider visco-elasticity have found that visco-elastic deformation inhibits the development of magmatic overpressures (Karlstrom et al., 2010; de Silva and Gregg, 2014) and viscous relaxation inhibits dike nucleation and growth (Jellinek and DePaolo, 2003). Therefore, the contribution of purely elastic thermal expansion around magmatic chambers or intrusions in the context of magma chamber rupture and dike initiation has not been previously addressed. Hence there is a gap in our understanding of how the elastic expansion and contraction of rocks around magma chambers, and the resulting plastic deformation in terms of the formation of brittle fracture (thermal cracking), develop as a result of temperature changes and crustal temperature gradients.

To address these issues, we conducted a numerical study to compare the elastic thermo-mechanically induced stresses of both mechanical and thermal loading on the crust around a magma chamber. In doing this we consider the influence of thermoelastic deformation around magma chambers and assess the impact on conditions leading to magma chamber failure, dike initiation and hence, potential eruptions.

2 - Methods

For the models, we solve the conductive heat transfer and elasticity equation using coupled mechanics within a Finite Element Method (FEM) 2D medium (e.g., Zienkiewicz, 1979; Deb, 2006). The geometric modeling, mesh discretization and numerical computations are carried out with COMSOL Multiphysics v5.5 software package (http://www. comsol.com, Tabatabaian, 2014). The magma chambers are modelled as cavities or holes with applied excess pressure (P_e) and temperature (e.g. Karaoğlu et al., 2016; Gudmundsson, 2011; Gerbault, 2012; Gerbault et al., 2012) embedded in a homogeneous crustal segment. We present models with both circular and elliptical magmatic geometries, which represent spherical and ellipsoidal chambers as are typical of ideal, and commonly modeled shapes, of magma chambers around the world (e.g. Gudmundsson, 2012; Chestler and Grosfils, 2013; Le Corvec et al., 2013; Caricchi et al., 2014). Although near-surface stress fields might be affected by topography, the primary focus of the presented models is on the stress differences caused by different boundary conditions applied only to the magma chambers and hence we use a flat topography in all models. The modelled crustal segment is 50 km in length and 40 km in depth. The magma

chambers are either circular with a radius of 2 km or elliptical with 8 km in length and 2 km in thickness, with a sill like geometry. The circular chamber has its roof at 3 km and the elliptical chamber at 4 km such that the depth of the center is the same for both geometries (Figure 1). We do not examine the influence of different depths or positions of the chambers although this topic has been discussed by Karaoğlu et al. (2020). The Young's modulus (E) of the host rock is 25 GPa. We use a constant typical value of Poisson's ratio (ν) of 0.25 (e.g. Gudmundsson, 2012) (Fig. 1).

We employ homogeneous thermal properties for the crustal segment for simplicity and in order to discern first order processes, although we acknowledge this is likely an oversimplification (Nabelek et al., 2012; Rodríguez et al., 2015). We use a value of 2 for thermal conductivity k [in W/(m*K)] (Whittington et al., 2009) in thermal steady state calculations. Considering the characteristics of the crustal segment; 850 for specific heat capacity C_p [in J/(kg*K)] and $3x10^{-6}$ for the coefficient of thermal expansion α [in 1/K] (Fig. 1) are selected to be used in Equation 2. The coefficient of thermal expansion for constituent minerals varies from around $1x10^{-6}$ up to around $30x10^{-6}$ 1/K (Huotari and Kukkonen, 2004), but since here we are interested in the bulk rock thermal expansion, we use a conservative value of 3×10^{-6} 1/K (Wong and Brace, 1979). It should also be noted that minerals such as quartz possess highly anisotropic thermal expansion coefficient depending on the axes of expansion (i.e., Meredith et al., 2001). This is at least part of the reason that quartz bearing rocks such as granite experience thermal crack damage when heated (Glover et al., 1995). We do not consider anisotropic thermal expansion in the following models, although the topic should be revisited once a basic understanding of the effects of isotropic thermal deformation has been gained.

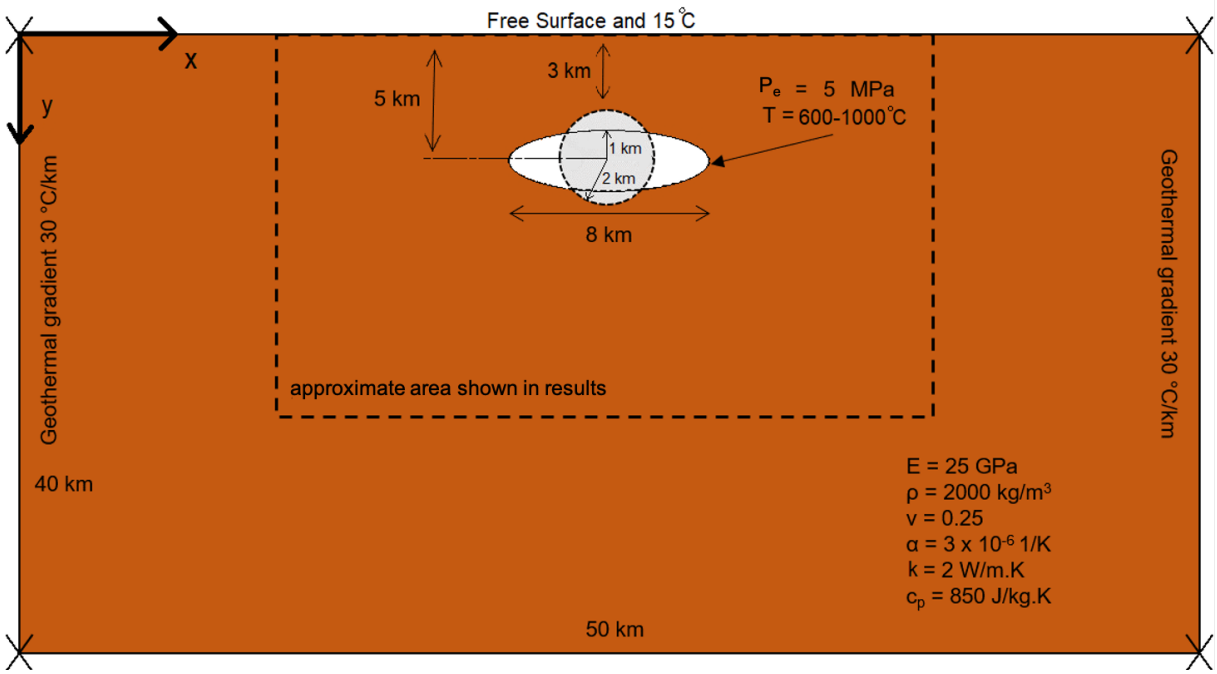

Figure 1. *Sketch of the model setups showing the geometrical relationship between a shallow magma chamber, either circular or elliptical, within the homogeneous crustal segment. In the models with a circular magma chamber the radius of the chamber is 2 km. In the models with a magma chamber with an elliptical geometry the chamber has a length of 8 km and a thickness of 2 km. The chamber is either pressurized with an internal overpressure of 5 MPa or a temperature at the margin of the chamber of either 600°C, 800°C or 1000°C or a combination of both internal pressure and temperature. There is an imposed geothermal gradient of 30°C/km within the model domain in the heat transfer and thermomechanical models. In the*

solid only models there is no temperature assigned to the model. The upper surface of the model is a free surface and/or also with a temperature of 15°C. To compare the solid and coupled models we performed one set of isothermal thermomechanical simulations where the chamber was with the same temperature as the upper surface, i.e. 15°C. The properties and size of the crustal segment are shown. The approximate area of interest is shown, which is the area exhibited in the model result outputs given later.

2.1 - Governing equations for the model set ups

When radiative heat transfer is neglected, a steady form of the equation solved in the *Heat Transfer in Solids* interface of COMSOL becomes:

$$\rho\, C_p\, \boldsymbol{u} \cdot \nabla T + \nabla \cdot \boldsymbol{q} = q_0 + Q_{ted} + Q \tag{3}$$

where ρ is density, C_p is specific heat capacity at constant stress, T is absolute temperature, $\boldsymbol{u}$ is a velocity vector of translational motion, Q represents additional heat sources, in this case from the magma chambers, and $\boldsymbol{q}$ is heat flux by conduction and defined as

$$\boldsymbol{q} = -k\, \nabla T \tag{4}$$

where k is thermal conductivity. Q_{ted} is a thermoelastic dampening that accounts for thermoelastic effects in solids. This is relevant only when heat transfer is coupled to solid mechanics and calculated by

$$Q_{ted} = -\boldsymbol{\alpha}\, T : \frac{dS}{dt} \tag{5}$$

where $\boldsymbol{\alpha}$ is the coefficient of thermal expansion, and S is the second Piola-Kirchhoff stress tensor.

In the "Solid Mechanics" interface of COMSOL the steady form of the equation of motion for linear elastic material is solved as follows:

$$0 = \nabla \cdot S + \boldsymbol{F}_v \tag{6}$$

$$S = S_{ad} + \boldsymbol{C} : \varepsilon_{el} \tag{7}$$

$$S_{ad} = S_0 + S_{ext} + S_q \tag{8}$$

$$\varepsilon_{el} = \varepsilon - \varepsilon_{inel} \tag{9}$$

$$\varepsilon_{inel} = \varepsilon_0 + \varepsilon_{ext} + \varepsilon_{th} + \varepsilon_{hs} + \varepsilon_{pl} + \varepsilon_{cr} + \varepsilon_{vp} \tag{10}$$

$$\varepsilon = \frac{1}{2}\left[(\nabla \boldsymbol{u})^T + \nabla \boldsymbol{u}\right] \tag{11}$$

In these equations $\boldsymbol{F}_v$is the volume force vector, $\boldsymbol{\varepsilon}$ is strain tensor, $\boldsymbol{C}$ is the constitutive tensor which is a function of Young's modulus (E) and Poisson's ratio (ν), and $\boldsymbol{u}$ is the displacement field. Also, ε_{el} is an elastic strain, ε_{inel} is an inelastic strain, ε_0 is initial strain, ε_{ex} is the external strain, ε_{hs} is a hygroscopic strain, ε_{pl} is a plastic strain, ε_{cr} is creep strain, ε_{vp} is a viscoplastic

strain, and ε_{th} is the thermal strain which is a function of temperature and thermal expansion coefficient and defined as

$$\varepsilon_{th} = \alpha\left(T - T_{ref}\right) \quad (12)$$

2.2 – Boundary conditions and parameters

To solve the aforementioned governing equations in the heat-transfer simulations only the boundary conditions related to heat transfer are necessary. However, for the coupled simulations of heat transfer and solid mechanics both the boundary conditions for the solid mechanics and heat transfer are required.

For the heat transfer and coupled thermomechanical part of the simulations, the temperature of the upper boundary of the computational domain (T_{up}) is set to 15°C; this is simply an approximation of the Earth surface temperature. The wall temperature of the magma chambers (T_{e1}) is assigned as either 600, 800 or 1000°C. We impose a temperature gradient (T_b) of 30°C/km to simulate increasing temperature with depth as follows:

$$T_b(y)[°C] = 30\ y[km] \quad (13)$$

For the solid mechanics part of the simulations; the upper boundary of the computational domain is defined as a free surface, i.e. the interaction with an area that cannot accommodate shear stress. A value of zero is defined as the normal stress and strain along both the lateral and bottom free boundaries and a fixed constraint is applied at the bottom boundary to avoid rigid body rotation. The models assume plane-strain conditions and are two-dimensional. Hence, the magma chambers are modelled as cavities with an infinite in-plane depth. We do not attempt to upscale the results to three-dimensions here and hence refer to the cavities as circular or elliptical. An excess pressure of 5 MPa is applied at the boundary of the magma chambers in all of the models.

To compare the results of the solid mechanics models with the thermomechanical coupled models we performed one set of isothermal coupled simulations where the magma chamber was the same temperature as the upper surface (i.e. 15°C) such that no thermal stress should be generated since there is was no temperature differential.

2.3 - Model mesh

We implemented a triangular mesh constructed by specifying the maximum element sizes on the boundaries of the computational domain and inside the domain separately. We did not mesh the interior of the magma cavity. The model mesh is set to 20 m and 75 m on the outer boundaries and the inside domain, respectively. On the magma cavity boundaries, the mesh was always less than 10 m. This scheme resulted in total of 1,495,214 and 1,493,782 elements for the circular geometry and elliptical magma geometry, respectively. The meshed models are shown in the supporting information.

3 - Results

3.1 - Mechanical models

In the suite of models shown in Figures 2 and 3 we simulated mechanical loading of the crustal segment by applying only an internal overpressure (P_e) of 5 MPa at the boundaries of the magma chambers. The resulting models are analysed in terms of the resulting amounts of minimum principal stress (maximum tensile stress) and von Mises shear stress. All of the models in this set are purely mechanical and not coupled with a heat field to generate thermal stress.

3.1.1 - Circular chamber

In these models the distributions of both the tensile and shear stresses are relatively homogenously located around the margin of the magma chamber. The level of tensile stress peaks at the lateral outer most margins, reaching a maximum of around 6 MPa at 5 km depth, and in the center directly above the chamber at the Earth's surface, reaching a maximum of around 3.8 MPa. These values are within the range of common tensile rock strengths (Amadei and Stephansson, 1997) and so rupture of the chamber walls is possible under such conditions. The general pattern of shear stress is the same although the levels of stress are higher, peaking at around 10 MPa at 5 km depth. The analysis at 5 km traverses the center of the magma chamber and hence these portions of the stress curves appear discontinuous (Figs. 2b and 2d). We make no attempt to infer the stress conditions within the magma body.

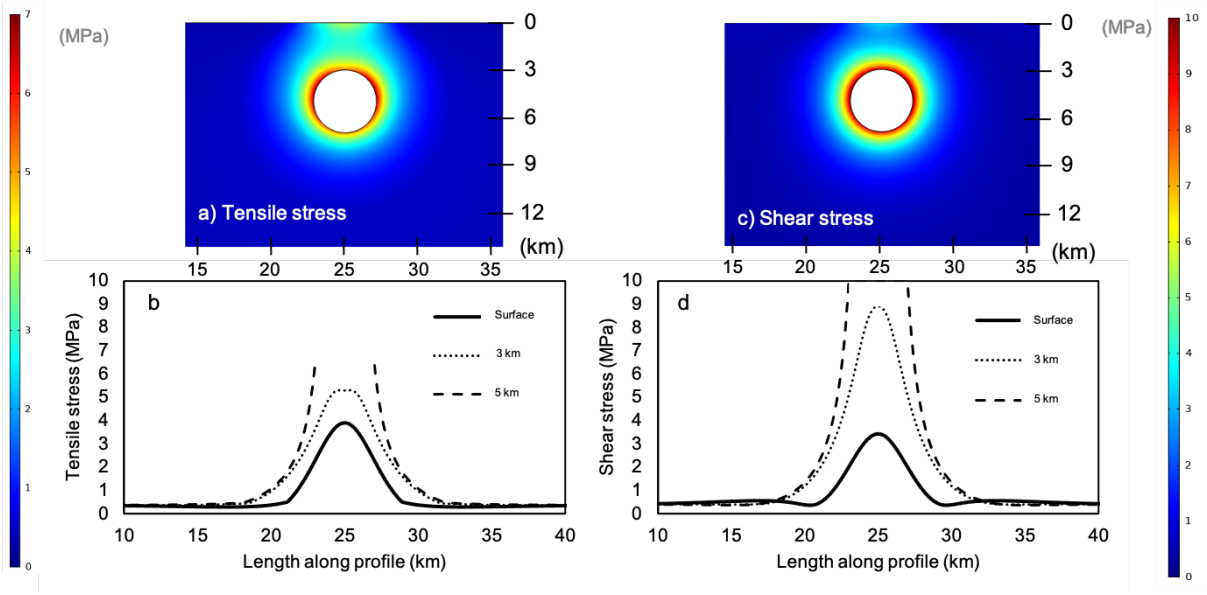

Figure 2. *2D mechanical numerical model setups of a 2 km radius circular magma chamber embedded in a homogeneous crustal segment 50 km in length (only 30 km of the profile are shown). The magma chambers, represented by cavities, are given an internal excess pressure of 5 MPa. Parts a and b show the distribution of tensile stress as function of depth, and part c and d show the distribution of von Mises shear stress.*

3.1.2 - Elliptical chamber

The results for an elliptical chamber show that both tensile and shear stresses concentrate at the margins of the magma chamber at depth, but focus centrally above the chamber at the surface. The magnitude of both the tensile and shear stresses is similar, between around 8-10 MPa at 5 km depth, and around 6 MPa near the surface. The levels of tensile stress are sufficiently high

to nucleate a magma-filled fracture and hence the models indicate that chamber rupture at the side of the chamber is likely under these conditions.

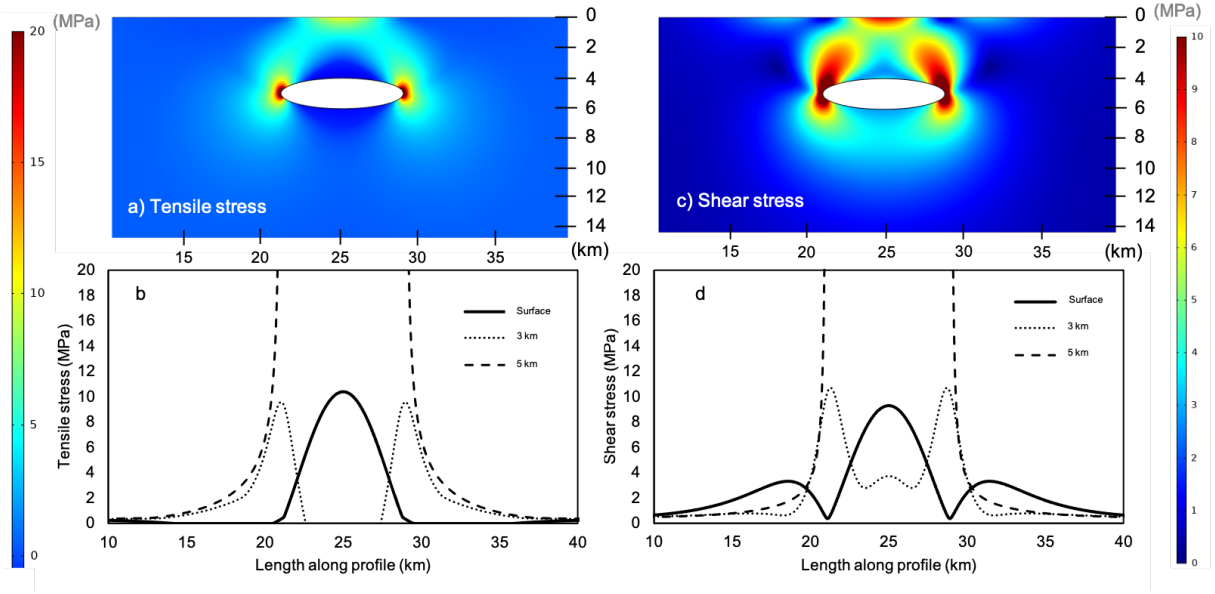

Figure 3. *2D mechanical numerical model setups of an 8 x 2 km magma chamber embedded in a homogeneous crustal segment 50 km in length (only between 10 and 40 km of the profile is shown). The magma chambers, represented by cavities, are given an internal excess pressure of 5 MPa. Parts a and b show the distribution of tensile stress as function of depth, and part c and d show the distribution of von Mises shear stress.*

3.2 - Heat transfer models

In Figures 4 and 5 we show the distribution of heat as a function of magma chamber temperature and geothermal gradient for both the circular and elliptical chambers. There is no mechanical coupling in these models and so only a temperature field output is generated. All of the models impose an assigned domain temperature gradient of 30ºC and with internal magma temperatures varying between 600°C, 800°C and 1000ºC. We plot the temperature field as a 2D surface and as curves of temperature vs distance along the profile at a depth of 5 km for each model.

3.2.1 - Circular chamber

As expected, heat is symmetrically distributed around the magma chamber with a pronounced peak in the central section above the roof. Temperature decreases with distance from the chamber and reaches the applied temperature at the domain boundaries. However, the central part of the domain remains with an elevated temperature of a few hundred degrees. Near the surface the temperature becomes elevated by a few tens of degrees, particularly in the regions directly above the magma chamber.

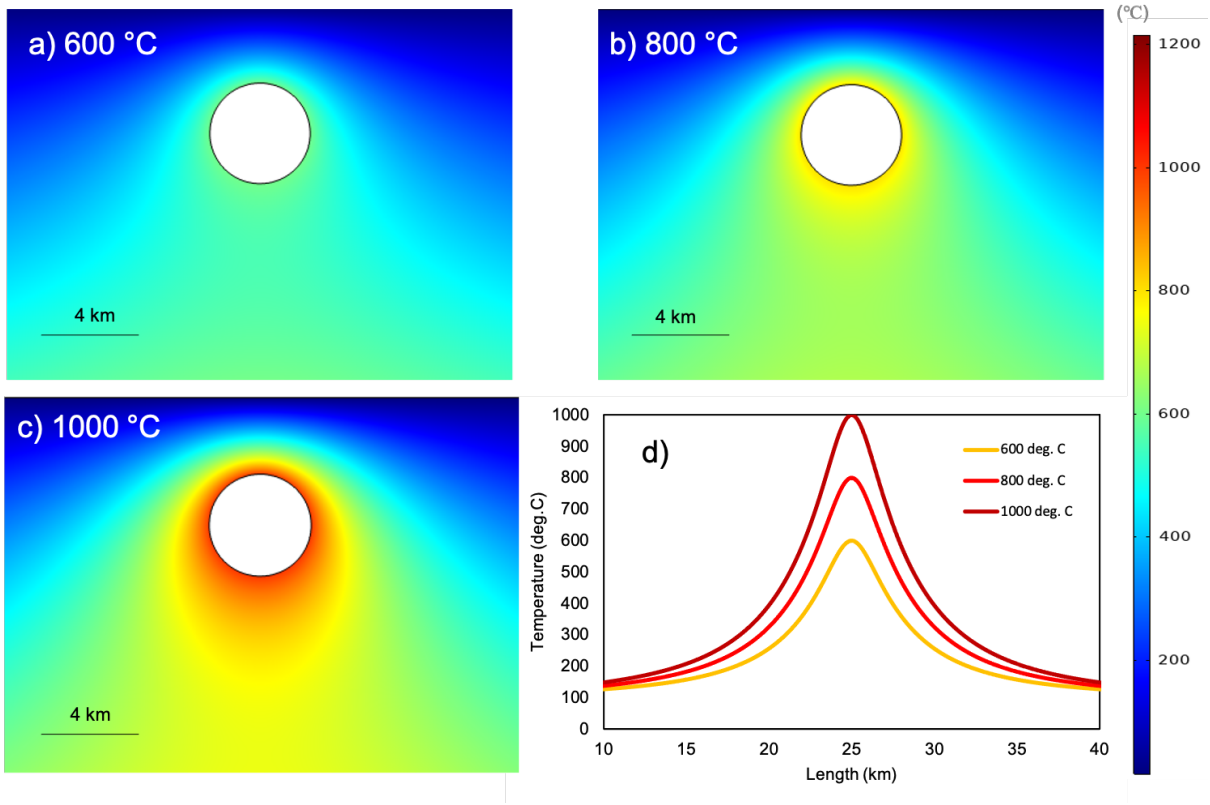

Figure 4. *Heat transfer models where the boundaries of the circular cavity are imposed a temperature of a) 600°C, b) 800°C and c) 1000°C and the model domain is set with a temperature gradient of 30°C/km. Part d gives the temperature distribution along the profile at a depth of 3 km, i.e. above the roof of the chamber. All profiles shown are the sections between 10 and 40 km along the profile length.*

3.2.2 - Elliptical chamber

The results from the simulations that model an elliptical chamber are very similar to the circular geometry, but the peak temperatures reflect the elongated geometry of the chamber. This results in higher temperatures along the length of the profile than compared with the circular geometry setup.

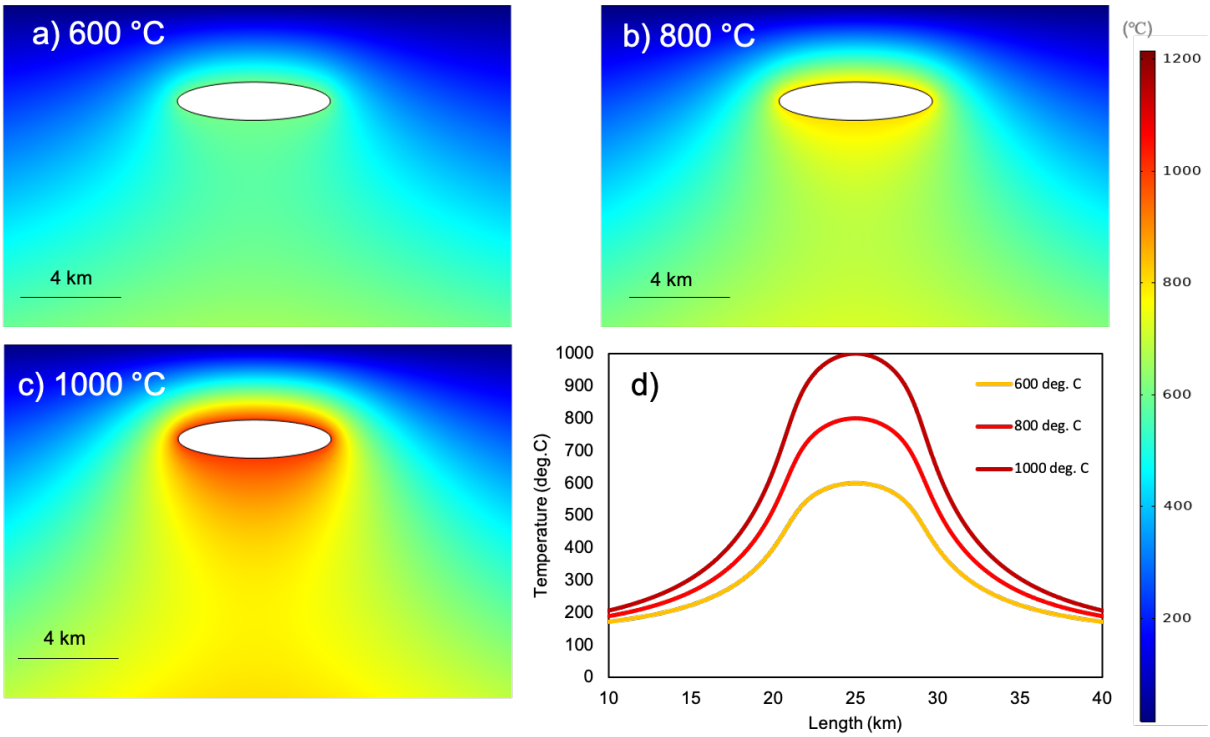

Figure 5. *Heat transfer models where the boundaries of the elliptical cavity are imposed a temperature of a) 600°C, b) 800°C and c) 1000°C and the model domain is set with a temperature gradient of 30°C/km. Part d gives the temperature distribution along the profile at a depth of 3 km, i.e. above the roof of the chamber. All profiles shown are the sections between 10 and 40 km along the profile length.*

3.3 - Coupled thermo-mechanical models

In Figures 6 and 7 we show the effect of coupled thermal and mechanical loading and the resulting crustal stress response around the two modelled magma chamber geometries at 1000ºC only. The coupled thermo-mechanical model results for all the temperatures are given in the supporting information but we focus here on only the maximum temperature (1000ºC) to highlight the main differences between the two model types. The loading in these models is generated from a competition between both the magmatic overpressure inside the magma chambers and from the thermal stress generated by the temperature imposed at the boundary of the magma chamber. The difference with the previous set of mechanical models (Figures 2 and 3) is that the temperature now exerts a mechanical response in the form of both the thermal expansion from the imposed temperature, and hence thermal expansion induced stressing, and loading from the internal magma pressure. As in the heat transfer models, we impose a temperature gradient of 30ºC/km in the y direction for the elevated temperature magma chamber models. The temperature profile generated in these thermo-mechanical models is hence identical to the purely thermal models given in the section 3.2. In Figures 6a, b, c and 7a, b, c we show the stress distribution from the magma chambers with an internal overpressure of 5 MPa but with an internal temperature of only 15ºC, so as to match the upper surface temperature and not generate any thermal stress. We hence effectively model the conditions already shown in Figures 2 and 3 but, importantly, this new model is thermo-mechanically coupled. This is an important test to ensure that the coupling does not generate undesired numerical effects. The resulting stress field, as expected, is similar to those given in Figure 2, for the circular chamber, and Figure 3, for the elliptical chamber. We can then compare directly the conditions of pressure

induced crustal stressing (Parts a, b and c of Figures 6 and 7) with both pressure and thermal induced stressing (Parts d, e and f of Figures 6 and 7).

3.3.1 - Circular chamber

The results of the thermo-mechanically coupled models that simulate an isothermal temperature condition (Figs. 6a, b, c) are almost identical to the mechanical loading models presented in section 3.1. Both the tensile and shear stresses peak at the center of the magma chamber and range from around 3 to 9 MPa depending on the depth. The stress field generated in the model that simulates a 1000°C chamber is quite different (Figs. 6d, e and f). The shear stresses both at the surface, and directly above the chamber at depth, again peak above the center of the magma chamber but now at a substantially higher level, between around 65 to 80 MPa. The tensile stress at the Earth's surface also again peaks at the projection of the center of the magma chamber but the level of stress is an order of magnitude higher at 85 MPa. The main difference in stress field occurs within the principal stress field at the margin of the chamber. The stress field at the margin is dominantly compressive and exhibits tensile peaks of between 10 and 20 MPa only at several kilometers away from the margin. These results indicate that the chamber could not rupture as there is no tension at its margin. However, there are abnormally high tensile stresses at the Earth's surface which are likely a model artefact, but if correct, would certainly lead to the formation of tension fractures.

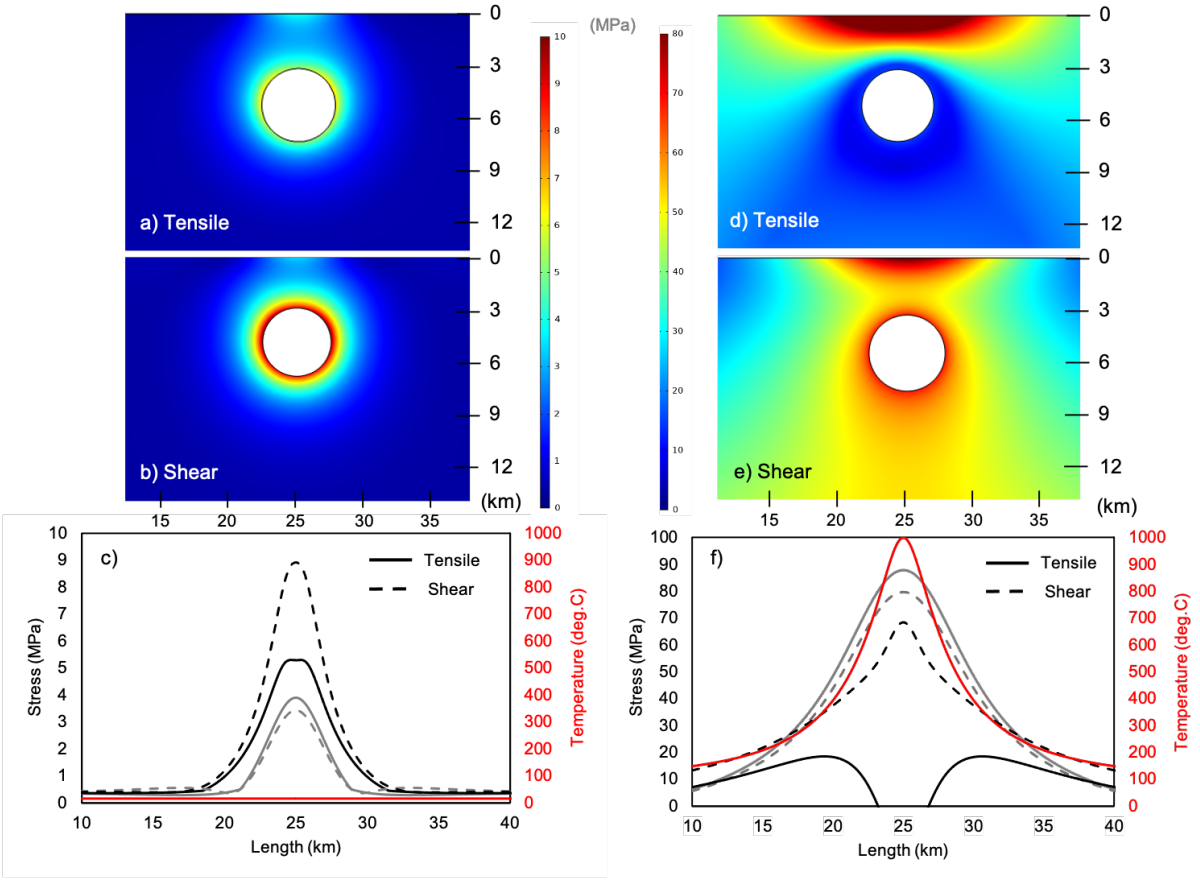

Figure 6. *Coupled thermomechanical models. The temperature field is shown as the red lines in each plot. The chamber in parts a, b and c is set to the same temperature as the upper surface, 15°C, such that there are no additional thermal stresses, whereas parts d, e and f exhibit both the imposed geothermal gradient and a 1000°C circular magma chamber. The black lines, in parts c and f, indicate measurements taken at 3 km depth, i.e. at the roof of the magma chamber,*

and the grey lines indicate measurements taken near the upper surface. Note: The scale of stress on the 1D plot is between 0 and 10 MPa in part c, but between 0 and 100 MPa in part f.

3.3.2 Elliptical chamber

The results from the isothermal condition thermo-mechanical models (Figs. 7a, b and c) are again broadly similar to those mechanical loading models presented in Section 3.1, as expected. At the earth's surface both the tensile and shear stresses peak above the center of the magma chamber, whereas at depth both stresses peak at its lateral sides. This indicates the chamber would rupture either in tension, forming a magmatic dike or sill, or in shear, forming a fault, at its most lateral extent. In these models it is perhaps more likely that a magma fracture would form since the tensile stress levels match or exceed the tensile strength of the host rocks, whereas the shear stress is not sufficiently high to match or exceed the compressive strength of most rock types (Gudmundsson, 2011).

As in the circular model case, if we again compare the most extreme temperature models (i.e. the chamber at 1000°C) with the isothermal case, for the elliptical magma geometry, it is possible to note the absence of the tensile stress concentrations at the margins of the chamber in the elevated temperature models. Since the stress concentrations are more pronounced in the elliptical model setups the absence of tensile stress in the elevated temperature models is notable (note Figure 7d). The maximum levels of tensile stress again peak several kilometers from the chamber and the dominant principal stress at the chamber margin is compressive.

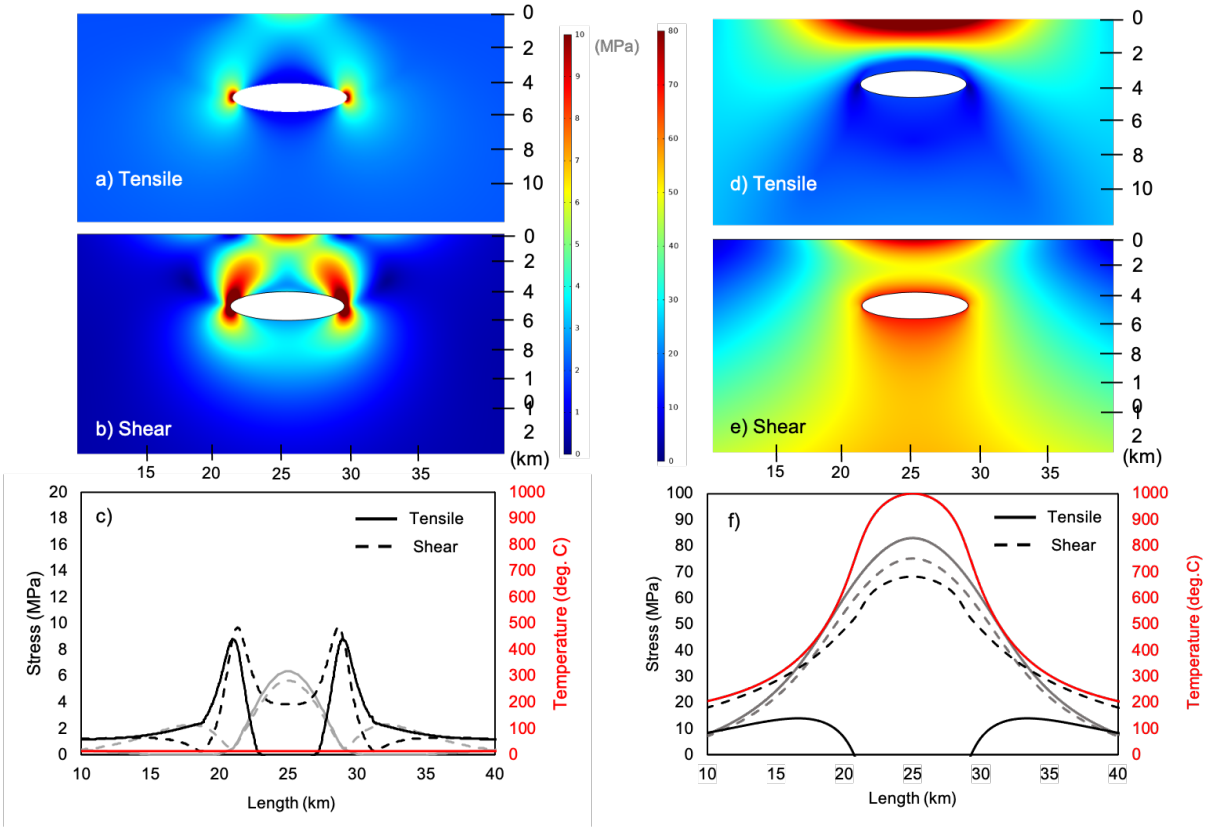

Figure 7. *Coupled thermomechanical models. The temperature field is shown as the red lines in each plot. In parts a, b and c the elliptical chamber is set to 15°C, the same as the upper surface temperature and hence no additional thermal stresses are produced, whereas parts d, e and f exhibit both the imposed geothermal gradient and a 1000°C elliptical magma chamber.*

The black lines, in parts c and f, indicate measurements taken at 4 km depth, i.e. at the roof of the magma chamber, and the grey lines indicate measurements taken near the upper surface. Note: The scale of stress on the 1D plot is between 0 and 20 MPa in part c, but between 0 and 100 MPa in part f.

4 - Discussion

To understand the influence of elastic thermo-mechanical stresses in crustal segments hosting hot but immature magma systems we compared stresses generated first in purely mechanical models and then with stresses generated in coupled thermo-mechanical models using steady-state solutions. In the suite of purely mechanical models we show that the maximum tensile stress is predominantly located at upper margin or roof of the circular chambers and at the sides of the elliptical magma chambers. The magnitude of these stresses is of the order of 10 MPa. Under such conditions the chamber would rupture and form a dike or sill as the level of tensile stress exceeds the local tensile strength of the host rock. These results are consistent with previously published data that consider elastic mechanical conditions (Thompson and Connolly, 1995; Gudmundsson, 2011). However, when the mechanical model is allowed to interact with a temperature field, modelled as a change in temperature that drives elastic thermal expansion, as in Figures 6 and 7, we are able to calculate the amount of stress resulting from the thermomechanical deformation. These thermo-mechanical models show that the magnitude of the tensile stress is influenced by internal magma pressure when there is no additional temperature condition (Figures 2 and 3), but by the combined effect of pressure and thermo-mechanical expansion when a temperature is applied to the chamber boundaries (Figures 6 and 7). This is demonstratable as the level of tensile stress is higher when the magma chamber and crustal segment were with isothermal (and hence no differential temperature or thermal stress) conditions, than when the chamber was assigned an elevated temperature (Figure 8). We find that when the magma chamber temperature is elevated, the principal stress field around the chamber margin becomes dominantly compressive in both magma chamber geometries tested (Figure 8). The zones of maximum tension then shift from being directly at the chamber margin to instead being several kilometers away from the chamber. This suggests that thermal expansion within the host rocks directly surrounding the chamber may inhibit the local development of tensile stress when temperatures increase above 600°C. Above these temperatures the level of both tensile and shear stresses increase but in the crustal segment several kilometers away from the chamber. In terms of the shear stress this result is as expected since thermal expansion generates compression and hence shear stresses (Fredrich and Wong, 1986), but that does not explain the increased levels of tensile stress at the surface. The latter may relate to free surface effects. However, in general the results indicate that if the crustal rocks surrounding a magma chamber can heat sufficiently over time, due, for example, to a new pulse of magma, then the level of total pressure required to rupture the chamber, and hence to nucleate magma-filled fractures, would need to be greater to compensate for the thermal expansion that inhibits the formation of tensile stress. We note that whilst the geometry of the chamber is important in controlling the localization or concentration of stresses, the temperature effects observed act similarly in both geometries tested. Hence the broad pattern of tensile stress reduction and transition to compression at the chamber margin with the addition of temperature is similar in both the circular and elliptical cases (Figure 8), although the levels of stress are different.

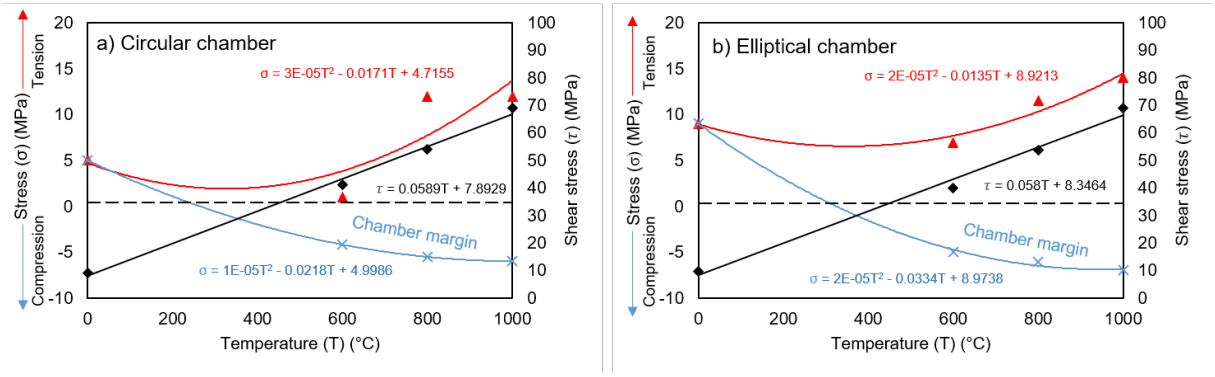

Figure 8. *Comparison of maximum shear (black diamonds), tensile (red triangles) and compressive (blue crosses) stresses as a function of temperature for the two magma chamber geometries, a) circular, b) elliptical. Linear and 2nd order polynomial best fits are shown. Note that the maximum level of tensile stress is adjacent to the magma chamber boundary at 0°C but peaks several kilometers away from the margin above 600°C. Instead, in both model geometries, the stress at the chamber margin is dominantly compressive at higher temperatures.*

Hence, we find that temperature induced elastic deformation of the host rocks surrounding a heated magma chamber induces two contrasting mechanical effects, 1) it induces high levels of shear stress; 2) it suppresses tensile stresses generated from the internal magma overpressure (Fig. 8). High levels of shear stress are produced as the overall stress field generated during thermal expansion is compressive, due in part to the expansion of the constituent grains in the rock mass (Browning et al., 2016). Compressive forces locally produce shear stress which, when sufficiently high, can also induce shear fracture in the form of thermal cracks (Fredrich and Wong, 1986; Browning et al., 2016). The generation of thermal crack damage may critically weaken the rocks surrounding a magma chamber and make future rupture easier, whether in shear (generating faults) or tension (generating magma-filled fractures). It has been shown that porosity reduces rock strength (Heap et al., 2014), and in this case the porosity, as cracks, may be generated through cyclic thermal cracking (Daoud et al., 2020).

Therefore, any tensile stresses generated by magmatic pressure may be effectively cancelled out by the thermal expansion of the host rock. As such, we may reconsider the requirement for magma chamber rupture introduced in Equation 1, and introduce a term that takes account for the expansion of the rocks surrounding the chamber due to heating:

$$P_l + P_e = \sigma_3 + T_0 \pm \Delta\sigma_T \quad (13)$$

where $\Delta\sigma_T$ is the additional or suppressed level of tensile stress induced from thermal expansion of the host rocks as a function of temperature increase (obtained from Figure 8). In Figure 8 we show the maximum level of shear and tensile stress as a function of temperature. Changes in temperature increase the level of shear stress, which is always highest at the chamber margins. Conversely, increases in temperature reduce the level of tensile stress located at the chamber margin and generate compressive stresses, but also increase the level of tensile stress several kilometers away from the chamber margin (Figures 6 and 7c). This indicates that both the spatial distribution of stresses, i.e. the stress field, and the level of stresses must be jointly considered in forecasting chamber rupture. Combining the model results and the effect of temperature in equation 13 suggests that failure would be most likely to occur if the rocks surrounding the chamber were sufficiently cold. These results suggest that chamber rupture would be favored during the initial phase of magma chamber replenishment and hence in a

relatively immature magma system. The effects of ductile or viscous deformation likely become important later on, when a magma system matures (de Silva and Gregg, 2014; Parisio et al., 2019). There may also be situations where competing forces, i.e. tension from magma pressure and compression from thermal expansion, act to combine and lower the critical stress level needed to fracture the host rock through mechanisms such as sub-critical cracking (Kemeny, 1991) or cyclic degradation (Heap et al., 2009), but such interactions are beyond the scope of our models.

The calculated drop in the tensile stresses around the chamber is of the same order of magnitude as the inferred tensile strength of the host-rocks. This suggests that, for any magmatic recharge event, the contribution of temperature increase alone may prevent magma chamber failure and the nucleation of dikes feeding eruptions during unrest. Under these conditions, other factors may play an important role in determining the likelihood of eruption. These include the presence of hot magma rich in volatiles (increasing P_e) and a delayed (viscous) response associated with the thermal expansion. In the latter case, it must be noted that the upper range of temperatures modelled could induce melting or a change from brittle to ductile rheology and as such the rocks could deform in a visco-elastic manner (Currenti and Williams, 2014; Degruyter and Huber, 2014; Gola et al., 2021). Visco-elastic deformation has been used to explain deformation signals at volcanoes (Del Negro, 2009; Castaldo et al., 2017) and some have suggested that such deformation mechanics may suppress the development of magmatic overpressures (de Silva and Gregg, 2014). In the models presented here we consider only the effects of elastic thermal deformation and hence do not consider the effect of visco-elastic deformation, although models that combine the two should be investigated in the future. We also do not consider thermal shock effects which require very rapid rates of heating or cooling (i.e. Van Otterloo et al., 2015). Essentially then, the models presented here, like all elastic or inelastic models, represent rapid processes such as stress concentration prior to or during failure. Over these timescales the influence of viscous deformation is likely much less. Crustal heat diffusion is a slow process and as such our results are likely more accurate near the boundaries of the magma chambers than for example at the Earth's surface, where we observe anomalously high stress in the coupled models. Also, over timescales of tens of years and more; viscous effects are certainly important and are also likely coupled with diffusive heat transfer in the crust which we also do not consider. It should also be noted that crustal stresses induced from magmatic injections, or replenished magma, are cyclic (Le Corvec et al., 2013) and any fracture damage induced, either through inflation (Heimisson et al., 2015) or thermal cracking (Browning et al., 2016; Daoud et al., 2020) is hence additive, although fracture healing or annealing may occur between cycles (Smith and Evans, 1984). Our models do not yet consider such additive damage, as well as the role of any thermal contraction around the magma bodies, from cooling, although future work aims to address this.

5 - Conclusions

We designed a suite of numerical models to investigate 1) the distribution of stress, through purely linear-elastic mechanical models, as a function of assumed crustal mechanical properties and mechanical crustal loading, 2) the distribution of heat in the crust, through purely heat-transfer models, as a function of assumed crustal thermal properties, and finally 3) combined thermo-mechanical models which took all of the relevant crustal material properties into account and simulated the elastic deformation from both thermal and mechanical loading.

It was found that crustal stress is related to both thermal expansion of rocks around hot magma chambers and loading from magmatic pressure inside the chamber. This is demonstrable

because when the temperature at the boundary of the magma chambers was increased the levels of crustal stress observed also increased (Figure 8).

We also find that purely mechanical models predict the rupture of magmatic bodies at the edges (or tips) of their lateral margins, but the thermo-mechanical models suggest that such rupture is more complicated as the amounts of tensile stress at the chamber margins are largely inhibited. Since the drop in the tensile stresses around the chamber is of the same order of magnitude as the inferred tensile strength of the host-rocks, thermal expansion due to magma injection may prevent the nucleation of magma-filled fractures and thus the development of dikes feeding eruptions during unrest. This situation is likely most relevant to immature magmatic systems that have recently been replenished by magma rather than long-lived mature systems. In mature systems other factors (e.g. volatiles, viscous host rock response) may become relevant in triggering chamber rupture and potential eruptions.

Acknowledgements

We thank the Editor Joel Ruch, reviewer Adelina Geyer and two anonymous reviewers for insightful comments which helped improve the manuscript. This study was supported by funds from Eskisehir Osmangazi Univeristy Numbers: 201715031 and 201715A215). OK was supported by The Scientific and Technological Research Council of Turkey (Postdoctoral Research Fellowship Programme). JB acknowledges support from Fondecyt award 11190143 and Fondap-Conicyt 15090013. Supporting data are included in an SI file; and may be obtained from JB (email: jbrowning@ing.puc.cl) and from http://doi.org/10.5281/zenodo.3601379

References

Amadei, B. and Stephansson, O., 1997. Rock stress and its measurement. Springer Science & Business Media.

Browning J, Drymoni K, Gudmundsson A (2015) Forecasting magma-chamber rupture at Santorini volcano, Greece. Scientific Reports 5:15785.

Browning J, Meredith P, Gudmundsson A (2016) Cooling-dominated cracking in thermally stressed volcanic rocks. Geophysical Research Letters 43(16):8417–8425.

Caricchi L, Annen C, Blundy J, Simpson G, Pinel V (2014) Frequency and magnitude of volcanic eruptions controlled by magma injection and buoyancy. Nature Geoscience 7(2):126–130.

Castagna A, Ougier-Simonin A, Benson PM, Browning J, Walker RJ, Fazio M, Vinciguerra S (2018) Thermal Damage and Pore Pressure Effects of the Brittle-Ductile Transition in Comiso Limestone. Journal of Geophysical Research: Solid Earth 123(9):7644-7660.

Castaldo, R., Gola, G., Santilano, A., De Novellis, V., Pepe, S., Manzo, M., Manzella, A. and Tizzani, P., (2017). The role of thermo-rheological properties of the crust beneath Ischia Island (Southern Italy) in the modulation of the ground deformation pattern. *Journal of Volcanology and Geothermal Research*, *344*, pp.154-173.

599 Currenti, G and Williams, C.A (2014). Numerical modeling of deformation and stress fields
600 around a magma chamber: Constraints on failure conditions and rheology, Physics of the Earth
601 and Planetary Interiors, Volume 226, 2014, Pages 14-27, ISSN 0031-9201
602
603 Chestler SR, Grosfils EB (2013) Using numerical modeling to explore the origin of intrusion
604 patterns on Fernandina volcano, Galápagos Islands, Ecuador. Geophysical Research Letters
605 40(17):4565–4569.
606
607 Daoud, A., Browning, J., Meredith, P., Mitchell, T. (2020). Microstructural Controls on
608 Thermal Crack Damage and the Presence of a Temperature-Memory Effect During Cyclic
609 Thermal Stressing of Rocks. *Geophysical Research Letters. 47, 19.*
610 https://doi.org/10.1029/2020GL088693
611
612 David C, Menéndez B, Darot M (1999) Influence of stress-induced and thermal cracking on
613 physical properties and microstructure of La Peyratte granite. International Journal of Rock
614 Mechanics and Mining Sciences 36(4):433–448.
615
616 Deb D (2006) Finite Element Method, Concepts and Applications in Geomechanics. PHI
617 Learning Private Limited, New Delhi.
618
619 Degruyter W, Huber C, Bachmann O, Cooper KM, Kent AJ (2016) Magma reservoir response
620 to transient recharge events: The case of Santorini volcano (Greece). Geology 44(1):23 –26.
621
622 Degruyter W, Huber C (2014) A model for eruption frequency of upper crustal silicic magma
623 chambers. Earth and Planetary Science Letters 403:117 –130.
624
625 Del Negro C, Currenti G, Scandura, D (2009) Temperature-dependent viscoelastic modeling of
626 ground deformation: application to Etna volcano during the 1993–1997 inflation
627 period. Physics of the Earth and Planetary Interiors 172(3-4):299–309.
628
629 Douglas, M. M., Geyer, A., Álvarez-Valero, A. M. & Martí, J. Modeling magmatic
630 accumulations in the upper crust: Metamorphic implications for the country rock. J. Volcanol.
631 Geotherm. Res. 319, 78-92 (2016).
632 https://doi.org/http://dx.doi.org/10.1016/j.jvolgeores.2016.03.008
633
634 Drymoni, K., Browning, J. and Gudmundsson, A., 2020. Dyke-arrest scenarios in extensional
635 regimes: Insights from field observations and numerical models, Santorini, Greece. Journal of
636 Volcanology and Geothermal Research, p.106854.
637
638 Fredrich JT, Wong, TF (1986) Micromechanics of thermally induced cracking in three crustal
639 rocks. Journal of Geophysical Research: Solid Earth 91(B12):12743–12764.
640
641 Gerbault M (2012) Pressure conditions for shear and tensile failure around a circular magma
642 chamber, insight from elasto-plastic modelling. Geological Society, London, Special
643 Publications 367(1):111–130.
644
645 Gerbault M, Cappa F, Hassani R (2012) Elasto-plastic and hydromechanical models of failure
646 around an infinitely long magma chamber. Geochemistry, Geophysics, Geosystems 13(3).
647

Glover PWJ, Baud P, Darot M, Meredith P, Boon SA, LeRavalec M, Zoussi S, Reuschle T (1995) α/β phase transition in quartz monitored using acoustic emissions. Geophysical Journal International, 120(3):775–782.

Grosfils EB (2007) Magma reservoir failure on the terrestrial planets: Assessing the importance of gravitational loading in simple elastic models. Journal of Volcanology and Geothermal Research 166(2):47–75.

Grosfils EB, McGovern PJ, Gregg PM, Galgana GA, Hurwitz M, Long SM, Chestler, SR (2015) Elastic models of magma reservoir mechanics: a key tool for investigating planetary volcanism. Geological Society, London, Special Publications 401(1):239–267.

Gudmundsson A (2011) Rock Fractures in Geological Processes. Cambridge University Press, Cambridge.

Gudmundsson A (2012) Magma chambers: Formation, local stresses, excess pressures, and compartments. Journal of Volcanology and Geothermal Research 237:19–41.

Gudmundsson, A., (2020). *Volcanotectonics: Understanding the Structure, Deformation and Dynamics of Volcanoes*. Cambridge University Press.

Gola, G., Barone, A., Castaldo, R., Chiodini, G., D'Auria, L., García- Hernández, R., Pepe S., Solaro G. and Tizzani P. (2021). A novel multidisciplinary approach for the thermo-rheological study of volcanic areas: The case study of Long Valley caldera. Journal of Geophysical Research: Solid Earth, 126, e2020JB020331. https://doi. org/10.1029/2020JB020331

Heap MJ, Vinciguerra S, Meredith, PG (2009) The evolution of elastic moduli with increasing crack damage during cyclic stressing of a basalt from Mt. Etna volcano. Tectonophysics 471(1-2):153–160.

Heap MJ, Xu T, Chen CF (2014) The influence of porosity and vesicle size on the brittle strength of volcanic rocks and magma. Bulletin of Volcanology 76(9):856.

Heimisson ER, Einarsson P, Sigmundsson F, Brandsdóttir B (2015) Kilometer-scale Kaiser effect identified in Krafla volcano, Iceland. Geophysical Research Letters 42(19):7958–7965.

Hickey J, Gottsmann J, Nakamichi H, Iguchi M (2016) Thermomechanical controls on magma supply and volcanic deformation: application to Aira caldera, Japan. Scientific Reports 6:32691.

Huotari T, Kukkonen I (2004) Thermal expansion properties of rocks: Literature survey and estimation of thermal expansion coefficient for Olkiluoto mica gneiss. Posiva Oy, Olkiluoto, Working Report 4:62.

Karaoğlu Ö, Browning J, Bazargan M, Gudmundsson A (2016) Numerical modelling of triple-junction tectonics at Karlıova, Eastern Turkey, with implications for regional transport. Earth and Planetary Science Letters 452:157–170.

Karaoğlu, Ö., Bayer, Ö., Turgay, M.B. and Browning, J., 2020. Thermomechanical interactions between crustal magma chambers in complex tectonic environments: Insights from Eastern Turkey. Tectonophysics, 793, p.228607.

Karlstrom L, Dufek J, Manga, M (2010) Magma chamber stability in arc and continental crust. Journal of Volcanology and Geothermal Research 190:249–270.

Kemeny JM (1991) November. A model for non-linear rock deformation under compression due to sub-critical crack growth. International Journal of Rock Mechanics and Mining Sciences and Geomechanics Abstracts 28(6):459–467.

Le Corvec N, Menand T, Lindsay J (2013) Interaction of ascending magma with pre-existing crustal fractures in monogenetic basaltic volcanism: an experimental approach. Journal of Geophysical Research: Solid Earth 118(3):968–984.

Maeda I (2000) Nonlinear visco-elastic volcanic model and its application to the recent eruption of Mt. Unzen. Journal of Volcanology and Geothermal Research 95(1-4):35–47.

Marsh BD (1989) Magma chambers. Annual Review of Earth and Planetary Sciences 17(1) 439–472.

Marti J, Ablay GJ, Redshaw LT, Sparks RSJ (1994) Experimental studies of collapse calderas. Journal of the Geological Society 151(6):919–929.

Meredith PG, Knight KS, Boon SA, Wood IG (2001) The microscopic origin of thermal cracking in rocks: An investigation by simultaneous time-of-flight neutron diffraction and acoustic emission monitoring. Geophysical Research Letters 28(10):2105–2108.

Mogi K (1958) Relations between eruptions of various volcanoes and the deformations of the ground surfaces around them. Bulletin of the Earthquake Research Institute 36:99–134.

Murase T (1963) Viscosity and related properties of volcanic rocks at 800°C to 1400°C. Journal of the Faculty of Science, Hokkaido University 7(1):487-584.

Nabelek, P. I., Hofmeister, A. M. & Whittington, A. G. The influence of temperature-dependent thermal diffusivity on the conductive cooling rates of plutons and temperature-time paths in contact aureoles. Earth Planet. Sci. Lett. 317-318, 157-164 (2012). https://doi.org/10.1016/j.epsl.2011.11.009

Novoa C, Remy D, Gerbault M, Baez JC, Tassara A, Cordova L, Cardona C, Granger M, Bonvalot S, Delgado F (2019) Viscoelastic relaxation: A mechanism to explain the decennial large surface displacements at the Laguna del Maule silicic volcanic complex. Earth and Planetary Science Letters 521:46-59.

Parisio, F., Vinciguerra, S., Kolditz, O. and Nagel, T., 2019. The brittle-ductile transition in active volcanoes. *Scientific reports*, *9*(1), pp.1-10.

de Silva SL, Gregg PM (2014) Thermomechanical feedbacks in magmatic systems: Implications for growth, longevity, and evolution of large caldera-forming magma reservoirs and their supereruptions. Journal of Volcanology and Geothermal Research 282:77–91.

Jellinek AM., DePaolo DJ (2003) A model for the origin of large silicic magma chambers: precursors of caldera-forming eruptions. Bulletin of Volcanology 65(5):363–381.

Rivalta, E., Corbi, F., Passarelli, L., Acocella, V., Davis, T. and Di Vito, M.A., 2019. Stress inversions to forecast magma pathways and eruptive vent location. Science advances, 5(7), p.eaau9784.

Rodríguez, C., Geyer, A., Castro, A. & Villaseñor, A. Natural equivalents of thermal gradient experiments. J. Volcanol. Geotherm. Res. 298, 47-58 (2015). https://doi.org/10.1016/j.jvolgeores.2015.03.021

Smith DL, Evans B (1984) Diffusional crack healing in quartz Journal of Geophysical Research: Solid Earth 89(B6):4125–4135.

Tabatabaian M (2014) COMSOL for Engineers. Mercury Learning and Information, Boston, USA.

Thompson AB, Connolly JA (1995) Melting of the continental crust: some thermal and petrological constraints on anatexis in continental collision zones and other tectonic settings. Journal of Geophysical Research: Solid Earth 100(B8):15565–15579.

Townsend M, Huber C, Degruyter W, Bachmann O (2019) Magma chamber growth during intercaldera periods: Insights from thermo-mechanical modeling with applications to Laguna del Maule, Campi Flegrei, Santorini, and Aso. Geochemistry, Geophysics, Geosystems 20(3):1574–1591.

Van Otterloo J, Cas RA, Scutter CR (2015) The fracture behaviour of volcanic glass and relevance to quench fragmentation during formation of hyaloclastite and phreatomagmatism. Earth-Science Reviews 151:79–116.

Whittington, A.G., Hofmeister, A.M. and Nabelek, P.I., 2009. Temperature-dependent thermal diffusivity of the Earth's crust and implications for magmatism. Nature, 458(7236), pp.319-321.

Wong TF, Brace WF (1979) Thermal expansion of rocks: some measurements at high pressure. Tectonophysics 57(2-4):95–117.

Zienkiewicz OC (1979) The Finite Element Method. McGraw–Hill, New York, p. 787.